Comparison of the NMR Spectroscopy Solution Structures of Pyranosyl-RNA and Its Nucleo-δ-peptide Analogue

Sergey Ilin,[a] Irene Schlönvogt,[b] Marc-Olivier Ebert,[b] Bernhard Jaun,[b] and Harald Schwalbe*[a, c]

The design of polymers that could mimic biomolecules in their ability to form assemblies similar to ribo- and deoxyribonucleic acids has become an attractive field of chemical research, and NMR spectroscopy has played a vital role in the determination of the three-dimensional structure of these newly designed nonnatural polymers. The structure of a self-complementary octamer duplex of pyranosyl-RNA (pRNA) has been determined by using NMR spectroscopy experimental data and an Xplor structure calculation protocol. The structure has been compared with the structure of a duplex formed by a designed nucleo-δ-peptide analogue of pRNA. The two duplexes assume one predominant conformation and show a high structural similarity. The conformation type of both structures agrees with those predicted based on qualitative conformational analysis and both structures show a good convergence toward the average torsion angles derived by NMR spectroscopy.

KEYWORDS:

NMR spectroscopy · nucleopeptides · pyranosyl-RNA · structural biology · structure elucidation

Introduction

In biological systems, ribo- and deoxyribonucleic acids constitute the building blocks for storage and transfer of genetic information. This function is dependent upon the reversible formation of duplex strands, stabilized by complementary Watson – Crick base pairing, and the ability to assemble monomers in specific sequences with high fidelity. The design of alternative polymers that could mimic biomolecules in their ability to form assemblies similar to ribo- and deoxyribonucleic acids has become an attractive field of chemical research.[1] One of the reasons for studying such alternatives is to understand the structural determinants of nucleic acid structure itself. In addition, the new synthetic oligomers provide a spatial arrangement of units able to self-pair, which may find applications in the biomedical, diagnostic fields and in materials science.

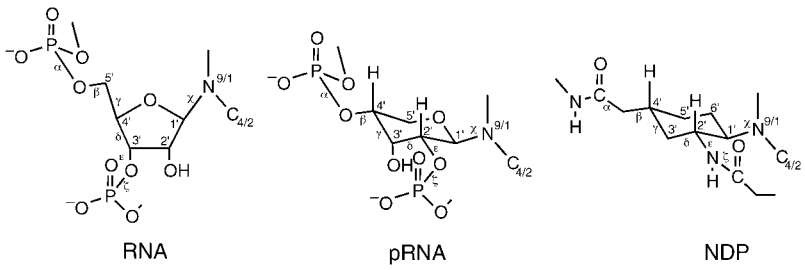

Scheme 1. *Constitution of RNA, pRNA, and nucleo-δ-peptides (NDP). The nomenclature for pRNA and NDP follows the IUPAC nomenclature for nucleic acids.[3]*

NMR spectroscopy has played a vital role in the determination of the three-dimensional structure of these newly designed nonnatural polymers.[2–12] Here, we report the NMR-spectroscopic determination of the structure of a self-complementary octamer duplex of pyranosyl-RNA (pRNA), pRNA-(C-G-A-A-T-T-C-G) (Scheme 1), and compare it to the NMR spectroscopy structure of a duplex formed by (1′*S*,2′*S*,4′*S*)-phba-nucleo-δ-peptide-(A-A-T-A-T), a nucleo-δ-peptide (NDP) that has been designed based upon the conformational insight derived from earlier studies of pRNA (Scheme 1; phba = the $[(HO)_2P(=O)-O-(CH_2)_3-C=O]$ radical attached to NDP).

pRNA nucleotides contain a six-membered pyranose sugar ring. In the oligomer, subsequent units are linked through a

[a] *Prof. Dr. H. Schwalbe, S. Ilin*
Department of Chemistry and
MIT/Harvard Center for Magnetic Resonance
at the Francis Bitter Magnet Laboratory
Massachusetts Institute of Technology
77 Massachusetts Avenue, Cambridge, MA 02139 (USA)
E-mail: schwalbe@nmr.uni-frankfurt.de

[b] *Dr. I. Schlönvogt, M.-O. Ebert, Prof. Dr. B. Jaun*
Laboratorium für Organische Chemie
Eidgenössische Technische Hochschule
Universitätsstrasse 16, 8092 Zürich (Switzerland)

[c] *Prof. Dr. H. Schwalbe*
Current address:
Center for Biological Magnetic Resonance
Institut für Organische Chemie
Goethe Universität Frankfurt
Marie-Curie-Strasse 11, N120-120
60439 Frankfurt (Germany)
Fax: (+49) 69-7982-9515

phosphodiester backbone that is bound to the C2′ and C4′ sugar centers. The most stable conformation of this oligomer is predicted to be the one in which the phosphate backbone assumes a *gauche-trans* conformation ($\zeta = 60^\circ$, $\alpha = 180^\circ$).[3] This idealized conformation leads to a linear strand, which is expected to form a quasilinear duplex arrangement stabilized by Watson – Crick base pairs.

In contrast, nucleo-δ-peptides are a new class of nucleic acid analogues, which contain a carbamoyl methyl group – peptide linkage in place of the phosphodiester backbone in pRNA and a cyclohexane instead of a pyranose ring.[13] The NDP structure shows a similar antiparallel duplex arrangement with Watson – Crick type base pairing as in pRNA. In NDP, however, the polymer backbone is more rigid than in pRNA since the peptide linkage in the backbone reduces the number of conformationally flexible single bonds from four to three. In addition, substitution of the pyranose ring by a cyclohexane ring further rigidifies the NDP structure.

Both, pRNA and NDP are chiral. In order to compare the conformation of the pRNA presented here with the NDP, the configuration of the NDP would have to be *R* at all centers (1′*R*,2′*R*,4′*R*). Since, for synthetic reasons, the NDP duplex studied in the previous work had the (1′*S*,2′*S*,4′*S*) configuration,[2] one of the two resulting structures has to be converted into its mirror image for direct comparison.

The present report extends the previous NMR-spectroscopic investigations by Schlönvogt et al.[3] for the pRNA sequence pRNA-(C-G-A-A-T-T-C-G) and by Schwalbe et al.[2] for the NDP sequence (1′*S*,2′*S*,4′*S*)-phba-nucleo-δ-peptide-(A-A-T-A-T). Model simulations and experimental studies of the pRNA demonstrated the formation of a quasilinear duplex with Watson – Crick base pairing and antiparallel strand orientation. From previous NMR spectroscopic studies and molecular-dynamics (MD) calculations, a slight deviation from the linear-idealized conformation was observed, which led to the proposal of a left-handed double helix.[13]

However, the previous structural investigations of the pRNA sequence deliberately did not include NMR experimental restraints to arrive at an NMR spectroscopy structure through a torsion angle simulated annealing protocol.[14] It is the focus of this report to use experimental NMR parameters, such as NOEs and coupling constants, to compute an NMR spectroscopy structure by using a simulated annealing protocol and to compare helical properties of the pRNA such as tilt, twist, and inclination with those of the NDP and naturally occurring ribonucleic acid in a duplex conformation.

Results and Discussion

Experiments and computation: pRNA

The 10 best structures with lowest energies for families I – IV were analyzed and compared in this report based on energy profiles of 280 ± 10 kcal mol^{-1}, 278 ± 10 kcal mol^{-1}, 270 ± 10 kcal mol^{-1}, and 280 ± 10 kcal mol^{-1} for families I – IV, respectively. Ensemble IV required a higher number of iterations due to the larger number of possible local minima. A summary of experimental distance restraints and structural statistics obtained are presented in Table 1.

Figure 1 shows four ensembles of overlaid structures. Families of structures I – IV all have the same starting conformation but different torsion-angle restraints, as given in Table 1. For the structure calculation resulting in the structures of family IV, the backbone torsion angles were left unrestrained.

The angles β and ε were restrained around 145° for β and -85° for ε based on experimental coupling constant data. These torsion angles deviate from the idealized structure of 180° for β

Table 1. *pRNA experimental restraints and structural statistics.*

Experimental restraints:	
NOE-derived distance restraints (total)	97
intraresidual	44
intrastrand	33
interstrand	20
hydrogen bond, base-planarity, and peptide-bond constraints	31
torsion-angle restraints	22
total experimental restraints	150
mean number per pRNA residue	19
Statistics of final structure:	
number of minimized structures	30
mean NOE deviation of convergent structures (> 0.2 Å)	0
torsion-angle deviation in convergent structures (> 5)	0
root mean square deviations from mean structure [Å]	
family I ($\pm 5^\circ$ β and ε restraints)	1.01
family II ($\pm 10^\circ$ β and ε restraints)	1.15
family III ($\pm 30^\circ$ β and ε restraints)	1.34
family IV (no β and ε restraints)	1.41

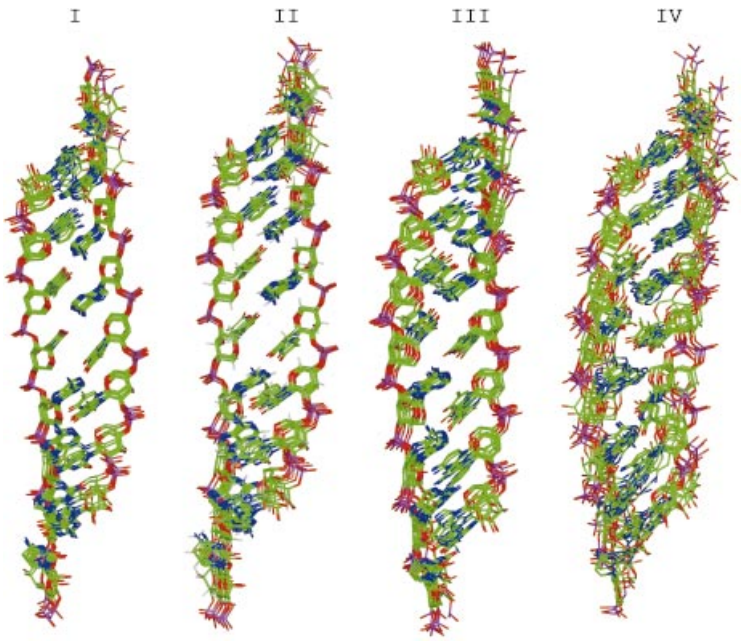

Figure 1. *Superposition of the ten best structures with different sets of experimental restraints. Torsion angle restraints of: I* $\beta = 145 \pm 5^\circ$ *and* $\varepsilon = -85 \pm 5^\circ$, *II* $\beta = 145 \pm 10^\circ$ *and* $\varepsilon = -85 \pm 10^\circ$, *III* $\beta = 145 \pm 30^\circ$ *and* $\varepsilon = -85 \pm 30^\circ$, *and IV: no torsion angle restraints of* β *and* ε. *The torsion angles* α *and* ζ *were left unrestrained in all simulations. The angle* χ *was restrained in all structures to* $\chi = -127 \pm 10^\circ$ *except for G8 (*$\chi = -97 \pm 10^\circ$*) and A4 (*$\chi = -110 \pm 10^\circ$*).*

and -60° for ε. In family I, the backbone torsion angles β and ε were restrained to $\pm 5^\circ$, close to the NMR spectroscopy error probabilities of $\pm 6^\circ$. In families II and III, the upper and lower bounds for these torsion-angle restraints were increased to $\pm 10^\circ$ and to $\pm 30^\circ$, respectively. A comparison of the statistical data presented in Tables 2 and 3, for ensemble IV on the one hand and for ensembles I – III on the other hand, clearly shows the importance of incorporating β and ε restraints in order to obtain a reasonable structure convergence, as shown in Figure 2.

Relaxing the restraint for the angles β, ε and χ as presented in Figure 1 did not alter the duplex conformation. However, the torsion angles shift slightly from the experimental values derived from the Karplus equation of ^3J(C,P) and ^3J(H,P) coupling constants for β. The torsion angles for the ensemble of structures I – IV are summarized in Table 2 and compared to the values obtained for the NDP structure calculation (Table 3). For the three restrained simulations, the midpoint of the restraining potential was set to 145°. In the calculated structure, the angle β varied from 151° when restraining $\beta = 145 \pm 5^\circ$, to 155° when restraining $\beta = 145 \pm 10^\circ$, to 159° when restraining $\beta = 145 \pm 30^\circ$. The lowest energy was obtained at 159°. The calculation, therefore, results in a deviation of 14° from the experimental angles predicted from ^3J(C,P) and ^3J(H,P) coupling constants. This deviation is lower than the deviation of 25° predicted by MD simulation.

For the ε angle, the midpoint was set to -85°. The agreement in the family of structures between experimental and calculated torsion angles in all three restrained simulations is much better and the calculated values are only a few degrees smaller than the angle derived from the coupling constants: -88° for $\varepsilon = -85 \pm 5^\circ$, -90° for $\varepsilon = -85 \pm 10^\circ$, and -91° for $\varepsilon = -85 \pm 30^\circ$. The phosphodiester backbone angles α and ζ were left unrestrained, since no experimental data were measured. In the $\varepsilon = \pm 30^\circ$ ensemble, α assumes angles around 86°, ranging from $67 - 96^\circ$, ζ assumes angles around -171° ranging from $-157 - -194^\circ$. The lower limit is observed for residue A4 and the higher limit for residue A3 in the duplex. Based on the previous NMR spectroscopy data,[3] the torsion angle χ was restrained to -127° for all residues in all calculations (families I – IV) with the exception of G8 and A4, which were set to -97° and -110°, respectively. For all torsion angles χ, an error of $\pm 10^\circ$ was assumed due to spin diffusion at mixing times above 40 ms on the cross-peaks to H–C(4′). The diagrams in Figure 2 show that the structures in families I – III obey these restraints well throughout the duplex,

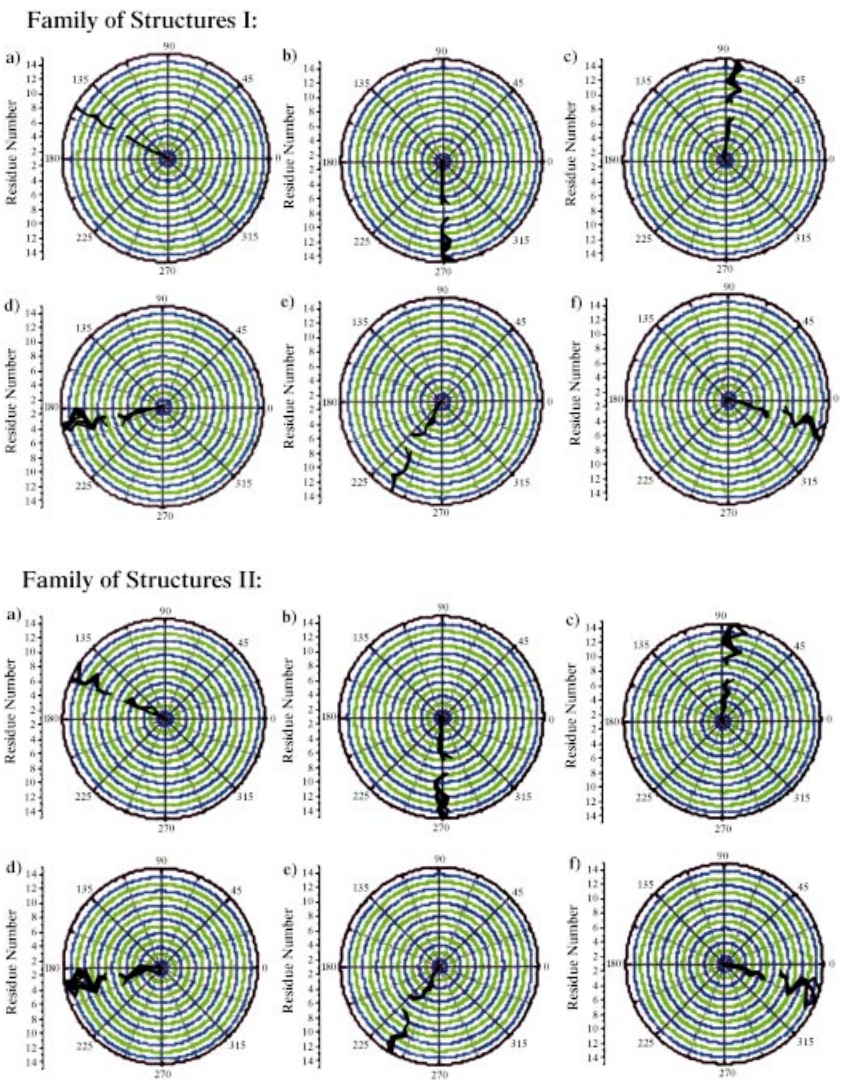

Figure 2. *Torsion angle distributions for all but the 3′-terminal residues in family of structures I – IV. Numerical values are listed in Table 2. a, b, c, d, e, and f correspond to angles β, ε, α, ζ, χ, and the helix twist, respectively. The data for each of the two strands is separated by a gap.*

Table 2. *Torsion angles for calculated simulated annealing structures in families I – IV in pRNA.*

	Family I	Family II	Family III	Family IV
α	$83.2 \pm 2.8^\circ$	$84.0 \pm 3.8^\circ$	$84.4 \pm 12.6^\circ$	$113.2 \pm 67.3^\circ$
β	$150.9 \pm 1.5^\circ$	$154.6 \pm 3.2^\circ$	$159.1 \pm 7.8^\circ$	$157.1 \pm 33.6^\circ$
ε	$-87.7 \pm 2.8^\circ$	$-89.8 \pm 4.0^\circ$	$-90.6 \pm 6.5^\circ$	$-102.3 \pm 33.4^\circ$
ζ	$-168.7 \pm 7.9^\circ$	$-167.9 \pm 8.0^\circ$	$-168.9 \pm 9.0^\circ$	$-156.4 \pm 50.9^\circ$

Table 3. *Torsion angles for the calculated simulated annealing family of structures in NDP.*

α	128.7 ± 1.3
β	167.8 ± 2.5
γ	169.9 ± 3.1
δ	175.8 ± 3.3
ε	123.4 ± 6.5
ζ	179.1 ± 7.6

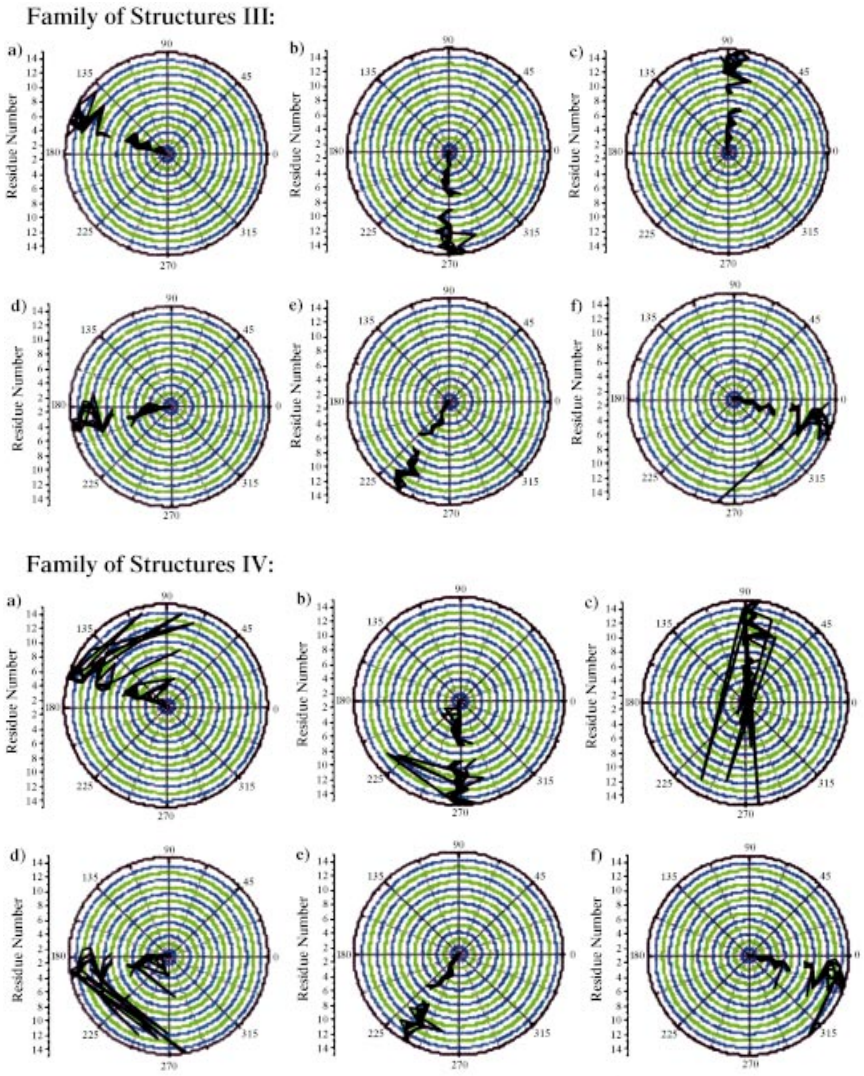

Figure 2. Continued

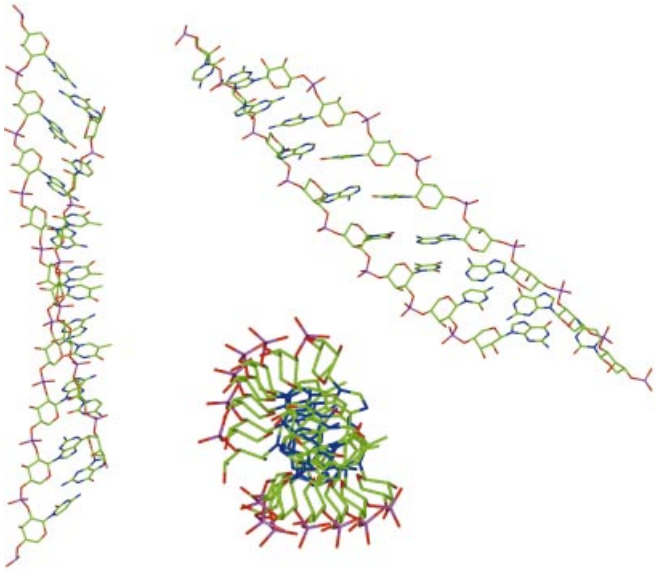

Figure 3. The pRNA duplex. From left to right: front, top, and side views.

while the unrestrained structures of family IV show higher fluctuations due to the presence of other local energy minima. However, based on energy and restraint violations, the best 10 structures out of 300 evaluated structures still yield a left-handed helix with strong inclination.

Helical properties for pRNA—Tilt

The structure of the pRNA duplex with lowest energy as shown in Figure 3 deviates from the linear idealized conformation. This causes the structure to form a left-handed double helix. MD simulations with and without fully energy minimized structure calculations have also predicted a left-handed helix conformation.[3] An interesting discrepancy between the experimentally derived pRNA structures presented here and those obtained by MD simulation is the direction of the bending in the duplex. The faces of the pRNA duplex are defined as concave and convex, as shown in Figure 4. The MD simulation

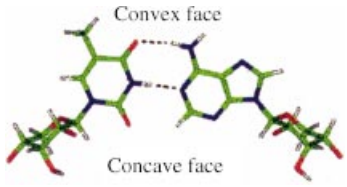

Figure 4. Definition of concave and convex face.

reveals a bend towards the concave side of the helix. In contrast, the structures in families I – III calculated in the simulated annealing protocol show an opposite bend towards the convex side in the higher restrained structure; then, the bend changes towards the concave side as the angle restraint is relaxed (III) or entirely omitted (IV), as in the MD simulation. This change in the bend of the ensembles is accomplished by a small angle variation of angle α (Table 2). Based on this observation, it appears that the MD bending might be an artifact of the simulation, probably due to the fact that torsion angles were left free to rotate with strong emphasis on the force fields whereas the NMR spectroscopy derived family of structures of the pRNA utilized experimental β, ε, and χ restraints. This further emphasizes the importance of experimental restraints to determine the backbone angle α in these oligomers.[15]

The family of structures I has an average unit twist of approximately 16°, which decreases with decreasing angular restraints to 15.6° for II, 14.7° for III, and 12.9° for IV. This demonstrates that experimentally defined restraints force the double strand to conform to the left-handed twist. Nevertheless, without including torsion-angle restraints in the calculation, the

structure, though more relaxed, still remains close to the restrained structure. The pRNA duplex shown deviates from the linear idealized conformation to form a left-handed double helix.

Helical properties for pRNA—Inclination

Inclination is defined as a measurement between the base plane projection onto the duplex plane and an axis perpendicular to the translation vector along the duplex (M. Egli et al., personal communication). Due to a strong inclination of approximately -50° as shown in Figure 5, bases on opposite strands are

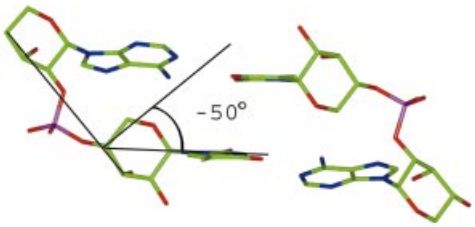

Figure 5. *Inclination of the pRNA duplex. Measurement is based on a method proposed by M. Egli et al. in a personal communication.*

positioned almost perfectly on top of each other and are presumably stabilized by interstrand stacking overlap as shown in Figure 6. Strong stacking interactions are observed for

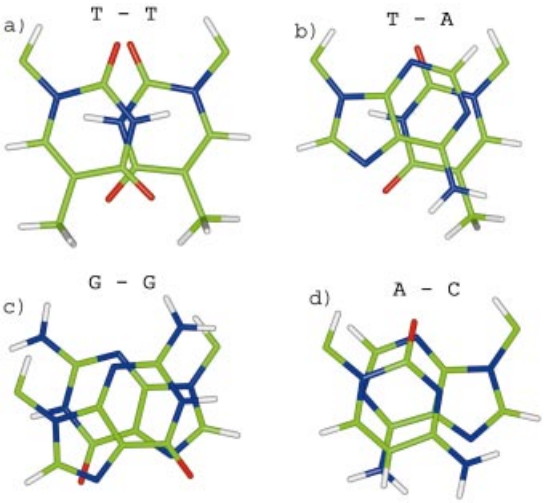

Figure 6. *Interstrand stacking: a) thymine – thymine, b) thymine – adenine, c) guanine – guanine, and d) adenine – cytosine.*

guanine – guanine and for thymine – adenine interstrand pairs. In contrast, thymine – thymine interstrand overlap is small and presumably does not contribute to stabilization through stacking interactions.

On the other hand, the intrastrand interactions between neighboring residues in the duplex are negligible. The strong inclination of -50° places subsequent residues on the same strand far apart from each other. The stacking distance between bases from opposite strands is in the range of 3.5 – 3.7 Å, depending on their position in the duplex (Figure 7). This distance is lower than the 4.5 Å predicted through model building for the idealized ribopyranosyl conformation. The discrepancy is due to a left-handed twisting of the duplex and strong base inclination.

Comparison of pyranosyl-RNA, NDP, and RNA

It is interesting to discuss the structural differences between naturally occurring A-form duplex RNA and nonnaturally occurring pRNA and NDP. Previous work has demonstrated that both pRNA and NDP have a stronger tendency to form antiparallel duplexes with Watson – Crick base pairing than RNA and that, in contrast to natural systems, they do not show purine – purine self-pairing of the reverse-Hoogsteen and Hoogsteen types. The A-type RNA duplex has 11 base pairs per turn. In contrast, pRNA consists of 23 base pairs per turn and NDP consists of 36 base pairs per turn. The large helical twist of 33° in RNA results in tight intrastrand stacking interactions and a rise per base pair of 2.6 Å. Bases in the $\pi-\pi$ stacking are separated on average by 3.4 Å or van der Waals allowed contact. Due to its small inclination of 20°, $\pi-\pi$ stacking occurs between intrastrand bases. In contrast, pRNA, which has a helical twist of 16°, is stabilized by interstrand base stacking, for which bases are separated by 3.5 – 3.7 Å on average with an inclination of -50°. NDP also has a strong inclination of -50°, yet bases are separated by 4.5 Å. Therefore, the structure of pRNA is more compact, as compared to the structure of NDP. As an example, if we consider 10 base pairs in the structure of pRNA and NDP, the overall rise would be 35 Å and 45 Å, respectively. The strong inclination in pRNA and NDP leads to a perfect alignment of two bases on opposite strands for $\pi-\pi$ base stacking. The peptide bond in the NDP backbone is constrained to a *trans* peptide configuration, which induces a more linear strand orientation. This is correlated with the smaller helicity compared to RNA and pRNA and is a consequence of the number of freely rotatable bonds in the acyclic portions of these molecules. The smaller change of the single-strand topography upon duplex formation due to the better structural preorganization may account for the higher stability of the NDP duplex as compared to pRNA and RNA duplexes. Also, the absence of repulsive electrostatic interactions in NDP will contribute to its

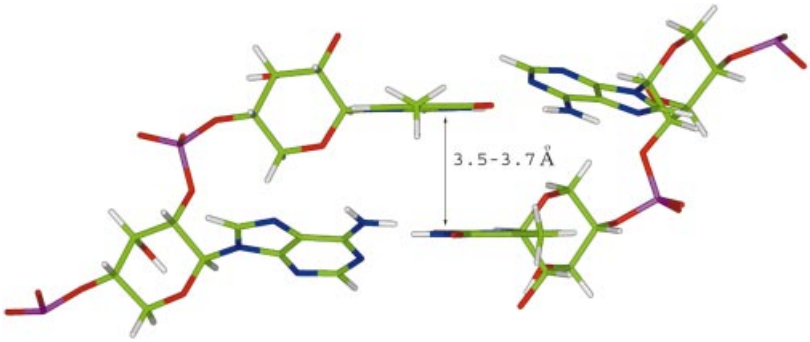

Figure 7. *Thymine – thymine interstrand base distance.*

high stability. pRNA would then appear to be in between the very stable NDP and the more flexible RNA duplex.

Conclusion

The conformations of the pRNA and NDP calculated with NMR spectroscopic restraints and molecular dynamics show that the two duplexes essentially assume one predominant conformation and that any other conformations have no statistical significance. The conformation type of both structures conforms to those predicted for the NDP and pRNA based on qualitative conformational analysis.[16–23] Both structures show a good convergence toward the average torsion angles derived by NMR spectroscopy. The comparison with the MD-derived structures of pRNA shows that, for these particular structures, calculations based on force fields alone, be it AMBER or CHARMM, might underestimate interactions such as interstrand $\pi-\pi$ stacking. Such stacking interactions are not as critical for RNA as for NDP and pRNA. Figure 8 shows the high structural similarity of the two oligomers. In conclusion, this study has examined a potentially natural nucleic acid pRNA and compared its structural attributes to its closest analogue NDP and natural ribonucleic acid.

Methods

Experimental restraints:

NOE Distance Restraints: For pRNA, a series of four NOESY spectra with mixing times of 40, 60, 80, and 150 ms, as well as a ROESY spectrum with a mixing time of 150 ms, were analyzed and relative distances were derived by integration of NOESY cross-peaks.[3] The results are listed in Table S1 in the Supporting Information based on the categories: weak (w) intensity 3 – 6 Å, medium (m) intensity 2.5 – 3 Å, and strong (s) intensity <2.5 Å. The NOE data summarized in Tables S1 and S2 have been used in the simulated annealing calculations. Table S2 in the Supporting Information summarizes the NOESY cross-peaks of exchangeable protons with equivalent distance estimation procedures as for nonexchangeable protons.

Dihedral Angle Restraints: The dihedral angles β and ε in the pRNA phosphodiester backbone were derived from analysis of coupling constants (J; Table S3 in the Supporting Information) by using the Karplus equations [Equations (1) and (2)]. Karplus coefficients determined by Haasnoot et al. for nucleic acids were used.[24] The Karplus parameterizations were further validated by Schlönvogt et al.[3] by comparison with experimental coupling constants measured in cyclophosphates of beta-D-ribopyranose-nucleosides.

$$^3J(H,P) = 15.3\cos^2\alpha - 6.2\cos\alpha + 1.5 \quad [Hz] \tag{1}$$

$$^3J(C,P) = 8.0\cos^2\alpha - 3.4\cos\alpha + 0.5 \quad [Hz] \tag{2}$$

Based on the experimental coupling constant $^3J(C(3'),P) = 8 \pm 1$ Hz for the pRNA, β may adopt two ranges ($\pm 141 \pm 6^\circ$). Combined with the four possible ranges ($+127 \pm 3^\circ$), ($-155 \pm 5^\circ$), ($-85 \pm 5^\circ$) and ($-7 \pm 3^\circ$) from measurement of $^3J(C(5'),P)$ and four possible ranges ($+137 \pm 7^\circ$), ($+103 \pm 7^\circ$), ($-117 \pm 3^\circ$) and ($-3 \pm 3^\circ$) from measurement of $^3J(H(4'),P)$, this results in a rather precise definition of $\beta \approx 145 \pm 6^\circ$.

Based on the Equation (1), the value of 7.4 ± 0.5 Hz observed for $^3J(H(2'),P)$ is consistent with four ranges for the angle ε: ($+122 \pm 3^\circ$), ($-152 \pm 3^\circ$), ($-89 \pm 3^\circ$), and ($-4 \pm 3^\circ$). Combined with dihedral angle ranges derived from $^3J(C(1'),P) = 10.6 \pm 0.5$ Hz and a small $^3J(C(3'),P)$ that has to be below the range given from the relatively narrow line width, the angle ε lies in the range to $-86 \pm 5^\circ$. The torsion angles β and ε calculated with Equations (1) and (2) deviate slightly from the values originally proposed by Schlönvogt et al. The deviations, however, are too small to effect the structure calculation. The angles α and ζ were determined based on β and ε experimental restraints, which confine α to -85° and ζ to -175°. Nevertheless, it is important to emphasize that these values were not considered in the simulated annealing structure calculations.

Conformational Analysis:

The structure of the pRNA oligomer was calculated starting from a randomized single-strand conformation. A modified simulated annealing protocol was used based on torsion-angle molecular dynamics with the Xplor 98.1 program.[14, 25, 26] The protocol was modified by adding an additional step of minimization with full Lennard – Jones nonbonding potentials and restrained dihedral terms at the end of the structural refinement. The slow cooling Cartesian molecular dynamics step was therefore omitted.

All the calculations were performed on SGI Origin 200 and/or SGI Octane computers. The simulated annealing protocol consisted of three minimization and two MD stages. The first stage consisted of 100 steps of standard preheating Powell minimization followed by two MD stages. The second preparation stage, performed in 60 ps, consisted of 4000 steps of high-temperature (20 000 K) torsion-angle dynamics with reduced nonbonding interac-

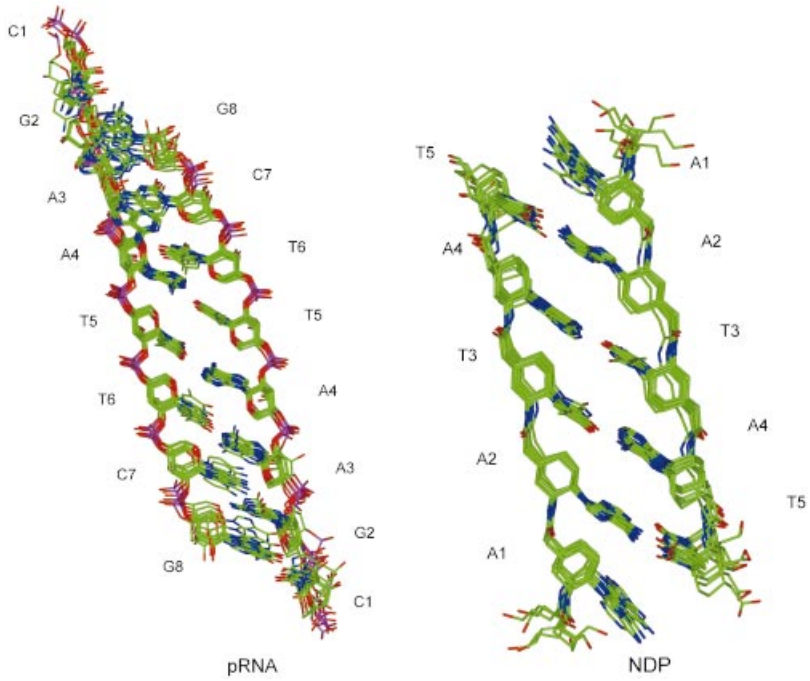

Figure 8. *Comparison of the family of structures simulated for pRNA and NDP.*

tions and hard-sphere repulsion by using a decreased force constant for heavy atoms and no force applied to interactions between hydrogen atoms. This was followed by a third stage, also performed in 60 ps, a slow-cooling process (20000 → 0 K) in 4000 steps. The nonbonding interactions were sealed back, while the NOE force was kept constant. In the last two stages, the structure was minimized, first by using the repel nonbonding potential for 2000 steps and then with the Lennard – Jones nonbonding potential for an additional 2000 steps. Pre- and post-Lennard – Jones structures were recorded.

The energy minimization was performed by using the adopted-basis Newton – Raphson (ABNR) method with the Charm 22 force field instead of the standard Powell method. The ABNR method shows greater ability to avoid entrapment in local minima by using second derivatives.

The force constants used in structure calculations for pRNA were based on standard nucleic acid derived structures[18] except for the sugar backbone. A distance of 1.9 ± 0.3 Å and a force constant of 150 kcal Mol^{-1} $Å^{-2}$ were used for the hydrogen bonds in base pairs. The values were identical to the values used for base pairing in oligonucleotides. In order to keep the bases planar, a force constant of 400 kcal Mol^{-1} $Å^{-2}$ was applied.

The standard CHARMM 22 force-field parameters for bond angles and length in the backbone were increased by a factor of two to ensure correct covalent geometry.

We thank the Massachusetts Institute of Technology, the Karl Winnacker-Foundation, the Fonds der Chemischen Industrie, and the Alfred P. Sloan Foundation for financial support. We thank Prof. Dr. A. Eschenmoser and Prof. Dr. G. Quinkert for fruitful discussions.

[1] K. Kirshenbaum, R. N. Zuckermann, K. A. Dill, *Curr. Opin. Struct. Biol.* **1999**, *9*, 530 – 535.
[2] H. Schwalbe, J. Wermuth, C. Richter, S. Szalma, A. Eschenmoser, G. Quinkert, *Helv. Chim. Acta* **2000**, *83*, 1079 – 1107.
[3] I. Schlönvogt, S. Pitsch, C. Lesueur, A. Eschenmoser, B. Jaun, R. Wolf, *Helv. Chim. Acta* **1996**, *79*, 2316 – 2345.
[4] J. Hunziker, H. J. Roth, M. Böhringer, A. Giger, U. Diederichsen, M. Göbel, R. Krishnan, B. Jaun, C. Leumann, A. Eschenmoser, *Helv. Chim. Acta* **1993**, *76*, 259 – 352.
[5] G. Otting, M. Billeter, K. Wüthrich, H. J. Roth, C. Leumann, A. Eschenmoser, *Helv. Chim. Acta* **1993**, *76*, 2701 – 2756.
[6] M. O. Ebert, B. Jaun, W. Pils, R. Micura, *Helv. Chim. Acta* **2000**, *83*, 2336 – 2343.
[7] D. Seebach, A. Jacobi, M. Rüping, K. Gademann, M. Ernst, B. Jaun, *Helv. Chim. Acta* **2000**, *83*, 2115 – 2140.
[8] T. Sifferlen, M. Rüping, K. Gademann, B. Jaun, D. Seebach, *Helv. Chim. Acta* **1999**, *82*, 2067 – 2093.
[9] K. Gademann, B. Jaun, D. Seebach, R. Perozzo, L. Scapozza, G. Folkers, *Helv. Chim. Acta* **1999**, *82*, 1 – 11.
[10] X. Daura, K. Gademann, B. Jaun, D. Seebach, W. F. van Gunsteren, A. E. Mark, *Angew. Chem.* **1999**, *111*, 249 – 253; *Angew. Chem. Int. Ed.* **1999**, *38*, 236 – 240.
[11] T. Hintermann, K. Gademann, B. Jaun, D. Seebach, *Helv. Chim. Acta* **1998**, *81*, 983 – 1002.
[12] S. Pitsch, R. Krishnamurthy, M. Bolli, S. Wendeborn, A. Holzner, M. Minton, C. Lesueur, I. Schlönvogt, B. Jaun, *Helv. Chim. Acta.* **1995**, *78*, 1621 – 1635.
[13] G. Karig, A. Fuchs, A. Busing, T. Brandsteller, S. Scherer, J. W. Bats, A. Eschenmoser, G. Quinkert, *Helv. Chim. Acta* **2000**, *83*, 1049 – 1077.
[14] E. G. Stein, L. M. Rice, A. T. Brunger, *J. Magn. Reson.* **1997**, *124*, 154 – 164.
[15] C. Richter, B. Reif, C. Griesinger, H. Schwalbe, *J. Am. Chem. Soc.* **2000**, *122*, 12728 – 12731.
[16] S. Pitsch, S. Wendeborn, B. Jaun, A. Eschenmoser, *Helv. Chim. Acta* **1993**, *76*, 2161 – 2183.
[17] R. Micura, M. Bolli, N. Windhab, A. Eschenmoser, *Angew. Chem.* **1997**, *109*, 899 – 902; *Angew. Chem. Int. Ed. Engl.* **1997**, *36*, 870 – 873.
[18] R. Micura, R. Kudick, S. Pitsch, A. Eschenmoser, *Angew. Chem.* **1999**, *111*, 715 – 718; *Angew. Chem. Int. Ed.* **1999**, *38*, 680 – 683.
[19] M. Beier, F. Reck, T. Wagner, R. Krishnamurthy, A. Eschenmoser, *Science* **1999**, *283*, 699 – 703.
[20] A. Eschenmoser, *Nucleosides Nucleotides* **1999**, *18*, 1363 – 1364.
[21] A. Eschenmoser, *Science* **1999**, *284*, 2118 – 2121.
[22] M. Bolli, R. Micura, A. Eschenmoser, *Chem. Biol.* **1997**, *4*, 309 – 320.
[23] F. Reck, H. Wippo, R. Kudick, M. Bolli, G. Ceulemans, R. Krishnamurthy, A. Eschenmoser, *Org. Lett.* **1999**, *1*, 1531 – 1534.
[24] C. A. G. Haasnoot, F. A. A. M. De Leeuw, C. A. Altona, *Tetrahedron* **1980**, *36*, 2783 – 2792.
[25] G. Parkinson, J. Vojtechovsky, L. Clowney, A. T. Brünger, H. M. Berman, *Acta Crystallogr. Sect. D* **1996**, *52*, 57 – 64.
[26] A. T. Brünger, *Xplor: A system for X-ray crystallography and NMR*, Yale University, New Haven, CT, **1996**.

Received: April 17, 2001
Revised version: July 23, 2001 [F 235]